КОМПЬЮТЕРНЫЕ ИССЛЕДОВАНИЯ
И МОДЕЛИРОВАНИЕ 2020 Т. 12 № 3 С. 575–595
DOI: 10.20537/2076-7633-2020-12-3-575-595

Ки&М

МОДЕЛИ В ФИЗИКЕ И ТЕХНОЛОГИИ

УДК: 532.516.5+536.24
MSC: 76D05, 80A20

Влияние силы плавучести на смешанную конвекцию жидкости переменной плотности в квадратной каверне с подвижной крышкой

А. А. Фомин[1,a], Л. Н. Фомина[2,b]

[1]Кузбасский государственный технический университет имени Т. Ф. Горбачева,
Россия, 650000, Кемерово, ул. Весенняя, д. 28
[2]Кемеровский государственный университет,
Россия, 650043, Кемерово, ул. Красная, д. 6

E-mail: [a] fomin_aa@mail.ru, [b] lubafomina@mail.ru

Получено 02.12.2019, после доработки — 01.03.2020.
Принято к публикации 11.03.2020.

В работе рассматривается задача стационарной смешанной конвекции и теплообмена вязкой теплопроводной жидкости в плоской квадратной каверне с подвижной верхней крышкой. Нагретая верхняя стенка каверны имеет температуру T_{H}, холодная нижняя — T_0 ($T_{\text{H}} > T_0$), а боковые стенки каверны теплоизолированы. Особенностью задачи является тот факт, что плотность жидкости может принимать произвольные значения в зависимости от величины перегрева крышки каверны. Математическая постановка включает в себя уравнения Навье–Стокса в переменных «скорость–давление» и баланса тепла, сформулированные с учетом несжимаемости течения жидкости и воздействия объемной силы плавучести. Разностная аппроксимация исходных дифференциальных уравнений выполнена методом контрольного объема. Численные решения задачи получены на сетке 501×501 для следующих значений параметров подобия: число Прандтля $\text{Pr} = 0.70$; число Рейнольдса $\text{Re} = 100, 1000$; число Ричардсона $\text{Ri} = 0.1, 1, 10$ и относительный перегрев верхней стенки $(T_{\text{H}} - T_0)/T_0 = 0,\ 1,\ 2,\ 3$. Достоверность полученных результатов подтверждена их сравнением с литературными данными. Представлены подробные картины течения в виде линий тока и изотерм перегрева потока. Показано, что увеличение значения числа Ричардсона (рост влияния силы плавучести) приводит к принципиальному изменению структуры течения жидкости. Также установлено, что учет переменности плотности жидкости приводит к ослаблению влияния роста Ri на трансформацию структуры течения. Это связано с тем, что изменение плотности в замкнутом объеме всегда приводит к возникновению зон с отрицательной плавучестью. Как следствие, конкуренция положительных и отрицательных объемных сил приводит в целом к ослаблению эффекта плавучести. Также проанализировано поведение коэффициентов теплоотдачи (числа Нуссельта) и трения вдоль нижней стенки каверны в зависимости от параметров задачи. Выявлено, что влияние переменности плотности на эти коэффициенты тем больше, чем большие значения при прочих равных условиях принимает число Ричардсона.

Ключевые слова: уравнения Навье–Стокса, вязкая жидкость, произвольное изменение плотности, теплообмен, смешанная конвекция, каверна с подвижной крышкой, численное моделирование

COMPUTER RESEARCH AND MODELING
2020 VOL. 12 NO. 3 P. 575–595
DOI: 10.20537/2076-7633-2020-12-3-575-595

Ки&М

MODELS IN PHYSICS AND TECHNOLOGY

UDC: 532.516.5+536.24
MSC: 76D05, 80A20

Effect of buoyancy force on mixed convection of a variable density fluid in a square lid-driven cavity

A. A. Fomin[1,a], L. N. Fomina[2,b]

[1]T. F. Gorbachev Kuzbass State Technical University,
28 Vesennaya st., Kemerovo, 650000, Russia
[2]Kemerovo State University,
6 Krasnaya st., Kemerovo, 650043, Russia

E-mail: [a] fomin_aa@mail.ru, [b] lubafomina@mail.ru

Received 02.12.2019, after completion — 01.03.2020.
Accepted for publication 11.03.2020.

The paper considers the problem of stationary mixed convection and heat transfer of a viscous heat-conducting fluid in a plane square lid-driven cavity. The hot top cover of the cavity has any temperature T_H and cold bottom wall has temperature T_0 ($T_H > T_0$), whereas in contrast the side walls are insulated. The fact that the fluid density can take arbitrary values depending on the amount of overheating of the cavity cover is a feature of the problem. The mathematical formulation includes the Navier–Stokes equations in the 'velocity–pressure' variables and the heat balance equation which take into account the incompressibility of the fluid flow and the influence of volumetric buoyancy force. The difference approximation of the original differential equations has been performed by the control volume method. Numerical solutions of the problem have been obtained on the 501×501 grid for the following values of similarity parameters: Prandtl number Pr = 0.70; Reynolds number Re = 100 and 1000; Richardson number Ri = 0.1, 1, and 10; and the relative cover overheating $(T_H - T_0)/T_0 = 0$, 1, 2, and 3. Detailed flow patterns in the form of streamlines and isotherms of relative overheating of the fluid flow are given in the work. It is shown that the increase in the value of the Richardson number (the increase in the influence of buoyancy force) leads to a fundamental change in the structure of the liquid stream. It is also found out that taking into account the variability of the liquid density leads to weakening of the influence of Ri growth on the transformation of the flow structure. The change in density in a closed volume is the cause of this weakening, since it always leads to the existence of zones with negative buoyancy in the presence of a volumetric force. As a consequence, the competition of positive and negative volumetric forces leads in general to weakening of the buoyancy effect. The behaviors of heat exchange coefficient (Nusselt number) and coefficient of friction along the bottom wall of the cavity depending on the parameters of the problem are also analyzed. It is revealed that the greater the values of the Richardson number are, the greater, ceteris paribus, the influence of density variation on these coefficients is.

Keywords: Navier–Stokes equations, viscous fluid, arbitrary change in density, heat transfer, mixed convection, lid-driven cavity, numerical simulation

Citation: *Computer Research and Modeling*, 2020, vol. 12, no. 3, pp. 575–595 (Russian).

Introduction

Mixed convection of fluid in the cavity due to both the shear force caused by the movement of the cavity wall and the buoyancy force due to thermal inhomogeneity of the cavity boundaries is manifested in many technical devices. One can cite the processes that occur during cooling of electronic devices, in heat exchangers, in handling of materials and growing of crystals, and many others as examples of the demonstrations of mixed convection. As a result, in order to understand the complex physical phenomena of mixed convection, numerous studies on this subject have been published in the literature.

It should be noted that the problem in question is considered in the Boussinesq approximation in the absolute majority of the studies (see, for example, [Iwatsu et al., 1993; Oztop, Dagtekin, 2004; Luo, Yang, 2007; Cheng, Liu, 2010; Sivakumar et al., 2010; Cheng, 2011; Malyshev et al., 2011; Mihailenko, Sheremet, 2018]). This approximation ignores density differences except where they appear in buoyancy term of the motion equation. The similarity parameters Pr, Re, Gr (or $\mathrm{Ri} = \mathrm{Gr}/\mathrm{Re}^2$) determine the solution in the scope of this model. As a rule, the main subject of the investigations is the effect of combinations of different values of these similarity numbers on heat transfer.

In particular, in [Iwatsu et al., 1993] numerical solutions of the Navier–Stokes and heat balance equations were obtained for broad range of the task parameters, namely: $0 \le \mathrm{Ra} \le 10^6$, $0 \le \mathrm{Re} \le 3000$, $\mathrm{Pr} \sim O(1)$, and walls aspect ratio $\sim O(1)$. The results clearly identified the major stream structures in various regimes of the parameters range. The flow features were similar to those of a usual lid-driven cavity of a 'cold' liquid when $\mathrm{Ri} \ll 1$. In opposite, many of the middle and bottom fluid portions of the cavity interior were stagnant when $\mathrm{Ri} \gg 1$. Moreover, the isoterms were nearly horizontal and vertically-linear temperature distributions were seen for this case in these cavity regions.

An interesting situation was investigated in [Oztop, Dagtekin, 2004], where not one but two opposite walls of the cavity were movable. Both the Ri number and the direction of the moving walls were found to affect fluid flow and heat exchange in the enclosure. For $\mathrm{Ri} < 1$ the effect of moving walls on heat transfer was the same when they moved in opposite directions, regardless of which side moved up, and it decreased when both moved up. In the case of $\mathrm{Ri} > 1$ and opposing buoyancy and shear forces, heat transfer was somewhat better due to the formation of secondary vortices on the walls and a counter vortex in the center.

The effect of temperature gradient orientation on the fluid flow and heat transfer in a lid-driven differentially heated square cavity was investigated in [Cheng, Liu, 2010]. Four cases were considered depending on the direction of temperature gradient. The study was performed for the following values of the similarity governing parameters: $\mathrm{Pr} = 0.7$ and $\mathrm{Ri} = 0.1$, 1, and 10. It was established that both the value of Ri and the direction of the temperature gradient affected the flow pattern, heat transfer processes and heat transport rates in the cavity. It was also found that the rate of heat exchange increased with decreasing Ri regardless of the orientation of the temperature gradient.

A large group of studies is devoted to research in caverns with partially heated walls. A typical representative of this line of research is work [Sivakumar et al., 2010]. The left wall was heated fully or partially to a higher temperature, whereas the right wall was maintained at a lower temperature in the investigation. Three different lengths of the heating portion and three different locations of it were utilized at the hot wall. It was concluded that the heat transfer rate increased with a decrease in the heating part and when this part was in the middle or upper part of the hot wall. Also, there are studies in the literature taking into account other factors complicating the process of mixed convection in a cavity. As a rule, complications concern the characteristics of the cavity itself, such as the inequality of the cavity sides [Kuznetsov, Maximov, 2008; Malyshev et al., 2011], the inclination of the cavity [Sivakumar et al., 2010] or, moreover, its rotation [Mihailenko, Sheremet, 2018]. A great attention is paid to the influence of additional process-complicating governing parameters in conjunction with

the influence of 'standard' process parameters such as Pr, Re, and Ri in these works. The values of additional parameters that maximally intensify the heat exchange process are determined.

Unexpected results were obtained in [Cheng, 2011], where a question under study was whether heat exchange would continuously increase with increasing Grashof and Reynolds numbers while preserving constant Richardson and Prandtl numbers. This question initiated the systematic study of the flow and heat transfer in a two-dimensional square cavity, where the flow was caused by the movement of the top cover in combination with the buoyancy force due to bottom heating. The investigations had shown that heat exchange continuously increased with increasing Re and Gr for Ri = 0.01, but not for $0.5 \leq \mathrm{Ri} \leq 100$. A sudden drop in the average Nu was also observed at Re = 713, 376, 248, 129, and 61 for Ri = 0.5, 1, 2, 10, and 100, respectively, due to changes in the flux and thermal structures, the heat transfer mechanism, and stream kinetic energy.

As for the works devoted to the study of essentially subsonic convective flows with an arbitrarily variable density, there are very few of them in the literature [Strelets et al., 1989; Becker, Braack, 2002; le Quere et al., 2005; Sun et al., 2010; Armengol et al., 2018]. The listed works are more theoretical, since the direction of research of subsonic flows with variable density is relatively new. The main task of these works is to substantiate the mathematical formulation, which does not take into account the dependence of fluid density on pressure. In other words, this statement does not describe the propagation of sound waves, which is the norm when modeling fluid flows with velocities much lower then the sound speed. However, results for comparisons can only be found in some of them [le Quere et al., 2005; Sun et al., 2010]. Unfortunately, all mentioned studies are related to the natural thermal convection in a closed cavity. The works devoted to the solution of the problem of mixed thermal convection of a liquid with an arbitrarily variable density in a closed region were not found in the literature.

From the above it follows that there is a lack of systematic studies of mixed thermal convection of a liquid with an arbitrarily variable density in closed areas. In this regard, the present work is devoted to studying the influence of the magnitude of buoyancy force in wide ranges of the Richardson number and fluid overheating on the mixed convection of the such liquid in a flat square lid-driven cavity.

1. Statement of problem

The problem of stationary incompressible flow of a viscous heat-conducting liquid in a gravity field in a flat square lid-driven cavity is considered. The upper lid of the cavity moves at a constant speed U_c, which is much less than the speed of sound of the liquid. It is assumed that the heating of the liquid can be arbitrary high and, as a consequence, the density of the fluid can arbitrarily change. On the other hand, it is also assumed that the specific heat at constant pressure C_p, viscosity μ and thermal conductivity λ of the liquid are constant. The top cover is heated to the temperature of T_{H}, the bottom cold wall has the temperature of T_0, side walls are thermally isolated. T_{H} can exceed T_0 several times in general. The flow structure scheme and boundary conditions are shown in Fig. 1.

Within the framework of the physical formulation of the problem, the system of governing equations in dimensional form will be as follows [Loitsyanskiy, 1995]:

$$\frac{\partial \varrho U}{\partial X} + \frac{\partial \varrho V}{\partial Y} = 0, \tag{1}$$

$$\varrho U \frac{\partial U}{\partial X} + \varrho V \frac{\partial U}{\partial Y} = -\frac{\partial P}{\partial X} + \mu \left(\frac{\partial^2 U}{\partial X^2} + \frac{\partial^2 U}{\partial Y^2} \right) + \frac{\mu}{3} \frac{\partial}{\partial X} (\mathrm{div}\mathbf{V}), \tag{2}$$

$$\varrho U \frac{\partial V}{\partial X} + \varrho V \frac{\partial V}{\partial Y} = -\frac{\partial P}{\partial Y} + \mu \left(\frac{\partial^2 V}{\partial X^2} + \frac{\partial^2 V}{\partial Y^2} \right) + \frac{\mu}{3} \frac{\partial}{\partial Y} (\mathrm{div}\mathbf{V}) - \varrho g, \tag{3}$$

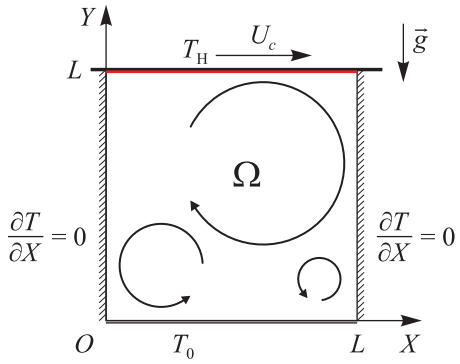

Figure 1. Scheme of flow in the lid-driven cavity with the warmed-up cover and the heat insulated side walls

$$C_p\varrho\left(U\frac{\partial T}{\partial X}+V\frac{\partial T}{\partial Y}\right)=U\frac{\partial P}{\partial X}+V\frac{\partial P}{\partial Y}+\lambda\left(\frac{\partial^2 T}{\partial X^2}+\frac{\partial^2 T}{\partial Y^2}\right)+N_D, \tag{4}$$

$$P=\frac{\varrho \mathrm{R}T}{m}. \tag{5}$$

Here U, V — horizontal and vertical velocity components respectively; ϱ — density, P — pressure, T — temperature, C_p — specific heat at constant pressure, μ — viscosity, λ — thermal conductivity, m — molar mass, R — universal gas constant, $\mathbf{V}$ — flow velocity vector, g — gravity acceleration module; N_D — the dissipation function:

$$N_D=\mu\left(\frac{\partial u}{\partial y}+\frac{\partial v}{\partial x}\right)^2+\frac{2\mu}{3}\left[\left(\frac{\partial u}{\partial x}\right)^2+\left(\frac{\partial v}{\partial y}\right)^2+\left(\frac{\partial u}{\partial x}-\frac{\partial v}{\partial y}\right)^2\right].$$

The characteristic values of the variables are introduced to estimate the orders of magnitude of the terms of the equations of system (1)–(4). Namely: value of L — for length, U_c — for velocity, T_0 — for temperature, ϱ_0 — for density, P_0 — for pressure. The characteristic density ϱ_0 is defined as the whole mass of the liquid in the cavity M_0 divided by the magnitude of the cavity volume $|\Omega|$. And the characteristic pressure P_0 is determined from the equation of state (5) when substituting there ϱ_0 and T_0. It is obvious that the characteristic density is constant because the cavity is closed, that is ϱ_0 does not depend on the value of the liquid heating.

Further transformation of the system of equations (1)–(5) will be carried out in the manner of [Strelets et al., 1989] taking into account the incompressibility of the fluid flow. Let T_a be the average temperature of the fluid in the cavity, that is

$$T_a=\frac{Q}{C_pM_0}, \tag{6}$$

where Q is the amount of heat of the whole liquid. In this case, the average pressure can be entered as follows:

$$P_a=\frac{\varrho_0 T_a \mathrm{R}}{m}. \tag{7}$$

On the other hand, it is convenient to introduce a hydrostatic pressure $P_h = P_h(Y)$ at the average temperature T_a, which is determined from the hydrostatic equation

$$\frac{dP_h}{dY}=-\varrho_h g. \tag{8}$$

Here $\varrho_h = P_h m/(\mathrm{R}T_a)$ according to equation (5). The solution of equation (8) is $P_h = \mathrm{const}\exp(-\beta Y)$, where $\beta = gm/(\mathrm{R}T_a)$. It is not difficult to get an estimation of β. For example, $\beta \sim 10^{-4}$ for air, that

is $\beta \ll 1$. In other words, the hydrostatic pressure varies very slightly with height, whence it follows that $P_h \approx P_a$, that is it can be accepted that const = P_a or $P_h = P_a \exp(-\beta Y)$. Accordingly, it can be written that $\varrho_h = P_h m/(\mathrm{R}T_a) = P_a m \exp(-\beta Y)/(\mathrm{R}T_a) = \varrho_0 \exp(-\beta Y) \approx \varrho_0$.

Since the liquid is generally in motion, it is convenient to introduce a decomposition of pressure into hydrostatic P_h and dynamic P_* components: $P = P_h + P_*$. Thus $\partial P/\partial X = \partial P_*/\partial X$ and $\partial P/\partial Y = -\varrho_h g + \partial P_*/\partial Y \approx -\varrho_0 g + \partial P_*/\partial Y$. On the other hand, the order of magnitude of dynamic pressure is $P_* \sim \varrho_0 U_c^2$ by Bernoulli's law, while the order of magnitude of hydrostatic one P_h is $P_a \sim \varrho_0 a^2$ where a is the speed of sound [Loitsyanskiy, 1995]. The flow in the cavity is hyposonic according to the condition of the problem under consideration, that is $U_c \ll a$ whence it follows that $P_* \ll P_h$. Therefore, the equation of state (5) can be rewritten approximately as

$$\varrho = \frac{P_a m}{\mathrm{R}T}. \tag{9}$$

Comparison of (7) and (9) allows to obtain that:

$$\varrho = \varrho_0 \frac{T_a}{T}, \tag{10}$$

that is density is inversely proportional to temperature in hyposonic heated (cooled) flows with variable density. As it was shown in [Strelets et al., 1989], the solutions of such approximate system of equations practically coincide with the solutions of the original Navier–Stokes system in the case $U_c \ll a$.

The formula for calculation T_a follows from equation of state (10) in the light of (6):

$$T_a = \frac{\int\limits_\Omega C_p \varrho T \, d\omega}{\int\limits_\Omega C_p \varrho \, d\omega} = \frac{\int\limits_\Omega \varrho_0 T_a \, d\omega}{\int\limits_\Omega \varrho_0 T_a \, T^{-1} \, d\omega} = \frac{\int\limits_\Omega d\omega}{\int\limits_\Omega T^{-1} \, d\omega},$$

that is

$$T_a = |\Omega| \left(\int\limits_\Omega T^{-1} \, d\omega \right)^{-1}.$$

Based on the foregoing, the equations of motion of the system (2)–(3) will take the following form:

$$\varrho U \frac{\partial U}{\partial X} + \varrho V \frac{\partial U}{\partial Y} = -\frac{\partial P_*}{\partial X} + \mu \left(\frac{\partial^2 U}{\partial X^2} + \frac{\partial^2 U}{\partial Y^2} \right) + \frac{\mu}{3} \frac{\partial}{\partial X} (\mathrm{div}\mathbf{V}), \tag{11}$$

$$\varrho U \frac{\partial V}{\partial X} + \varrho V \frac{\partial V}{\partial Y} = -\frac{\partial P_*}{\partial Y} + \mu \left(\frac{\partial^2 V}{\partial X^2} + \frac{\partial^2 V}{\partial Y^2} \right) + \frac{\mu}{3} \frac{\partial}{\partial Y} (\mathrm{div}\mathbf{V}) + \left(1 - \frac{T_a}{T} \right) \varrho_0 g. \tag{12}$$

As for the work of the pressure forces in the heat balance equation, it is converted as follows:

$$U \frac{\partial P}{\partial X} + V \frac{\partial P}{\partial Y} = U \frac{\partial P_*}{\partial X} + V \frac{\partial P_*}{\partial Y} - V \varrho_0 g.$$

Taking into account that the estimate $g \sim U^2/L$ is valid for naturally convective flows, the order of magnitude of the components of the heat balance equation will be as follows:

- the convective transfer $\sim C_p \varrho_0 T_0 U_c/L \sim \varrho_0 a^2 U_c/L$;
- the work of the pressure forces $\sim \varrho_0 U_c^3/L$;
- the heat diffusion $\sim C_p \varrho_0 T_0 U_c/(\mathrm{Re}\,\mathrm{Pr}\,L) \sim \varrho_0 a^2 U_c/(\mathrm{Re}\,\mathrm{Pr}\,L)$;
- the dissipation function $\sim \varrho_0 U_c^3/(\mathrm{Re}\,L)$.

The estimations contain the following similarity parameters: Reynolds number $\mathrm{Re} = \rho_0 U_c L/\mu$, Prandtl number $\mathrm{Pr} = C_p \mu/\lambda$. Therefore, one can neglect the work of pressure forces and the dissipative function for the case $U_c \ll a$. It should be explained here that these estimates are valid for significant temperature changes in the study area when they are comparable to the reference value of the temperature T_0. Otherwise, the work of pressure forces cannot be neglected due to the fact that, strictly speaking, the temperature difference should be used for the estimates but not the temperature itself.

As a result, the heat balance equation will be as follows:

$$C_p \varrho \left(U \frac{\partial T}{\partial X} + V \frac{\partial T}{\partial Y} \right) = \lambda \left(\frac{\partial^2 T}{\partial X^2} + \frac{\partial^2 T}{\partial Y^2} \right).$$

The problem is solved in a dimensionless form and dimensionlessness is performed as follows: $X = x\,L$, $Y = y\,L$, $U = u\,U_c$, $V = v\,U_c$, $\varrho = \rho\,\varrho_0$, $P_* = p_* \varrho_0 U_c^2$, $T = T_0 + \theta(T_H - T_0)$. Accordingly, the system of governing equations will have the following form:

$$\frac{\partial \rho u}{\partial x} + \frac{\partial \rho v}{\partial y} = 0, \tag{13}$$

$$\rho u \frac{\partial u}{\partial x} + \rho v \frac{\partial u}{\partial y} = -\frac{\partial p_*}{\partial x} + \frac{1}{\mathrm{Re}} \left(\frac{\partial^2 u}{\partial x^2} + \frac{\partial^2 u}{\partial y^2} \right) + \frac{1}{3\mathrm{Re}} \frac{\partial}{\partial x} (\mathrm{div}\, \boldsymbol{\upsilon}), \tag{14}$$

$$\rho u \frac{\partial v}{\partial x} + \rho v \frac{\partial v}{\partial y} = -\frac{\partial p_*}{\partial y} + \frac{1}{\mathrm{Re}} \left(\frac{\partial^2 v}{\partial x^2} + \frac{\partial^2 v}{\partial y^2} \right) + \frac{1}{3\mathrm{Re}} \frac{\partial}{\partial y} (\mathrm{div}\, \boldsymbol{\upsilon}) + \mathrm{Ri} \frac{\theta - \theta_a}{1 + \delta_\mathrm{T} \theta}, \tag{15}$$

$$\rho u \frac{\partial \theta}{\partial x} + \rho v \frac{\partial \theta}{\partial y} = \frac{1}{\mathrm{Pr}\,\mathrm{Re}} \left(\frac{\partial^2 \theta}{\partial x^2} + \frac{\partial^2 \theta}{\partial y^2} \right); \tag{16}$$

with conditions at the borders of the research area (see Fig. 1):

the bottom wall: $u = v = 0,\ \theta = 0;$
the top cover: $u = 1,\ v = 0,\ \theta = 1;$
the side walls: $u = v = 0,\ \partial\theta/\partial x = 0.$

Here $\boldsymbol{\upsilon}$ is a dimensionless vector of velocity. It should be noted that the problem formulation (13)–(16) contains the following similarity parameters: Reynolds and Prandtl numbers Re and Pr accordingly, Richardson number $\mathrm{Ri} = \delta_\mathrm{T} g L/U_c^2$, and the relative overheating of the cavity top cover $\delta_\mathrm{T} = (T_\mathrm{H} - T_0)/T_0$.

The statement of the problem is completed using the equation of state (10) reduced to the dimensionless form:

$$\rho = \frac{1 + \delta_\mathrm{T} \theta_a}{1 + \delta_\mathrm{T} \theta}, \tag{17}$$

where $\theta_a = (T_a - T_0)/(T_\mathrm{H} - T_0)$ is the average relative overheating of the liquid.

It is easy to see that the volumetric force in the equation of motion for the vertical component of the velocity (15) can be both positive and negative due to the fact that there is a double inequality $0 < \theta_a < 1$. Therefore, the cavity area is divided into zones in which $\theta < \theta_a$ and $\theta > \theta_a$ in the light of the continuity of distribution of the flow overheating from zero (at the bottom wall) to unity (at the cavity cover). Thus, there are always zones with both positive and negative buoyancy when considering convective flows of liquids with a variable density in a closed region in the field of mass force. This conclusion is the main difference between the present mathematical formulation of the problem and that stated in the framework of the Boussinesq approximation.

An analysis of the equation of state (17) indicates that in zones $\theta < \theta_a$ an increase in δ_T leads to an increase in the density of the liquid ρ, ceteris paribus. Conversely, in the $\theta > \theta_a$ zones, an increase

in δ_T leads to a decrease in the liquid density. In other words, the similarity parameter of the relative overheating δ_T characterizes the degree of differentiation of the inertial properties of the liquid: the larger δ_T, the greater is the difference in the density of the liquid in the heated and cold zones of the fluid flow. As a result, the zeroing out of this parameter (and, as a consequence, the zeroing out of the $\operatorname{div}\boldsymbol{v}$) means that the Boussinesq approximation is used. It should be noted, that parameter δ_T also affects the value of the buoyancy force. However, here, as in the Boussinesq approximation, the buoyancy of the flow is primarily determined by the magnitude of the Richardson number.

2. Numerical method and code validation

The problem (13)–(17) is solved numerically by using a finite-difference relaxation technique. For this purpose, the original differential equations (13)–(16) are transformed to a non-stationary form. As for the first kind boundary conditions at the cavity cover, they also take the corresponding non-stationary form. Namely, the velocity and the relative overheating of the cover smoothly increase from zero to unity at initial times to ensure the stability of the numerical algorithm.

The technique of splitting in physical processes is applied to solve the continuity and motion equations at each time step [Belotserkovskii et al., 1975; Fomin, Fomina, 2015]. Herewith two modifications of the technique are used: 1) on the first step of splitting, the pressure is taken into account from the previous time layer and implicit difference schemes are used for the movement equations; 2) on the second step of splitting, the Neumann problem is formulated for the increment of pressure δp_*, which is equal to a difference of pressure p_* on the current and previous time layers. The field of relative flow overheating θ is recalculated for every time level on the basis of the newly calculated velocity field. And finally, the density field ρ is recalculated through the new overheating field using equation (17). The procedure is repeated until the solution becomes completely stationary.

Difference approximation of the differential equations is carried out by the control-volume method with fifth-order power-law scheme of second-order accuracy in space and first-order accuracy in time [Patankar, 1980]. In all calculations uniform grids are used with an identical step h along both coordinate axes. The resulting systems of algebraic linear equations with respect to numerical vectors $\mathbf{u} = \{u_{ij}\}$, $\mathbf{v} = \{v_{ij}\}$, $\Delta\mathbf{p} = \{\Delta p_{ij}\}$, and $\boldsymbol{\theta} = \{\theta_{ij}\}$ are solved by the implicit iteration line-by-line recurrence method of the second order, accelerated in Krylov subspaces [Fomin, Fomina, 2011; Fomin, Fomina, 2017]. Stationary flow characteristics are considered to be found when condition:

$$\frac{\left\|\mathbf{u}^n - \mathbf{u}^{n-1}\right\|_1 + \left\|\mathbf{v}^n - \mathbf{v}^{n-1}\right\|_1}{\Delta t \left\|\boldsymbol{v}^n\right\|_1} < 10^{-5}$$

is satisfied. Here superscript n is an index of a time level, Δt is a time step which is defined from the formula $\Delta t = C \min(h, \operatorname{Re} h^2)$, where C is Courant number. The optimal value of $C = 32$ has been determined from the results of computational experiments. Also, numerical experiments have shown that the overheating field and, accordingly, the density field stabilize most quickly. Therefore, a special condition for control of stabilization of the relative overheating field (density) is not used.

The problem for the following parameters: $\mathrm{Pr} = 0.7$, $\mathrm{Re} = 1000$, $\mathrm{Ri} = 3$, $\delta_T = 3$ has been solved with various grid partitions of the domain in order to determine the optimal difference grid. It has been found that for $h \leqslant 1/500$ the profiles of both components of velocity u and v, relative flow overheating θ, and dynamic component of pressure p_* are practically identical to each other (see Fig. 2). It is easy to see that the first norms of the relative differences of the vectors of the profiles of the flow parameters shown in the figure for grids with steps $1/500$ and $1/1000$ do not exceed 0.3%.

Also, in order to optimize the grid for different mesh coverings of the computational domain, a number of flow characteristics have been calculated, such as Nusselt number Nu along the top and bottom walls of the cavity and modified coefficient of friction C_f^* along the bottom wall. It is not

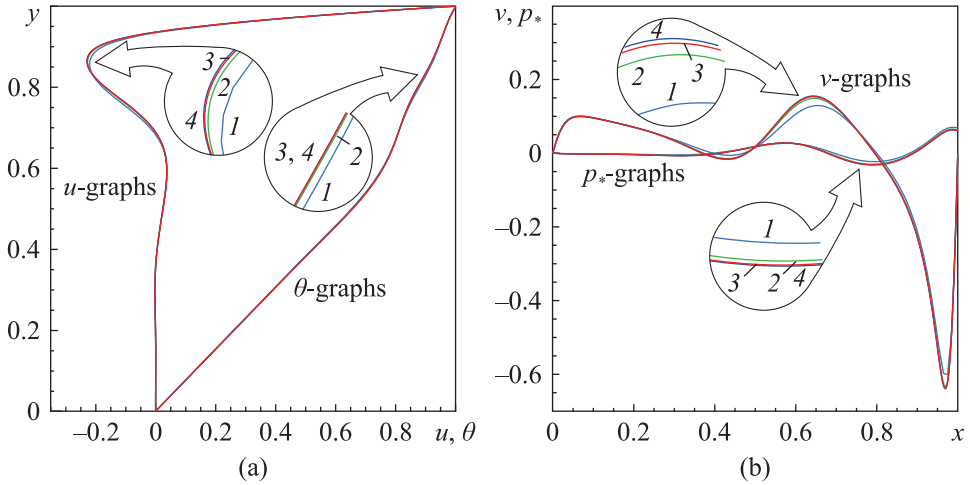

Figure 2. Evaluation of grid independency for (a) u-component of velocity and relative overheating θ at $x = 0.5$, (b) v-component of velocity and dynamic pressure p_* at $y = 0.9$. Grid is: 1 — 101×101, 2 — 251×251, 3 — 501×501, 4 — 1001×1001. Computation parameters are: Re = 1000, Ri = 10, Pr = 0.7, and $\delta_T = 3$

difficult to obtain computational expressions for these characteristics using their standard definitions and the nondimensionalization system adopted in this paper [Loitsyanskiy, 1995; Abu-Nada et al., 2007; Fomin, Fomina, 2018]:

$$\mathrm{Nu} = -(\partial\theta/\partial n)_w \quad \text{and} \quad C_f^* = C_f \mathrm{Re}/2 = (\partial u/\partial y)_w.$$

Here $\partial/\partial n$ is the outward pointing derivative with respect to the wall, subscript 'w' denotes 'on the cavity wall'. The advantage of C_f^* over C_f is that the modified coefficient of friction doesn't depend on Reynolds number Re.

Computation errors of the Nu and C_f^* are given in the table. The relative errors of the parameters have been calculated in relation to their values for the grid step of 1/1000. It is clearly seen, that the grid step of $h = 1/500$ is sufficient to calculate these parameters with reasonable accuracy. As a result, all the solutions of the problem were received for this grid step.

One interesting detail should be noted here: the grid independence of the solution according to the average Nusselt number Nu_{avr} on the top cover is achieved at a grid step of 1/50. While, to achieve independence of the solution from the grid with the same accuracy, but according to the local

Table 1. Extreme and average values of the stream parameters for the set of grid steps at Re = 1000, Ri = 10, Pr = 0.7, $\delta_T = 3$

Grid step	1/50	1/100	1/250	1/500	1/750	1/1000
Nu_{max} at $y = 1$	5.143	6.432	7.702	8.254	8.450	8.550
	39.84%	24.76%	9.91%	3.46%	1.16%	0.0%
Nu_{avr} at $y = 1$	1.356	1.321	1.304	1.303	1.303	1.306
	3.83%	1.15%	0.15%	0.23%	0.23%	0.0%
Nu_{min} at $y = 0$	–1.288	–1.303	–1.308	–1.308	–1.308	–1.308
	1.55%	0.41%	0.06%	0.01%	0.0%	0.0%
Nu_{avr} at $y = 0$	–1.274	–1.295	–1.304	–1.306	–1.306	–1.304
	2.30%	0.69%	0.00%	0.15%	0.15%	0.0%
$C_{f\,min}^*$ at $y = 0$	–0.00663	–0.00571	–0.00483	–0.00465	–0.00460	–0.00457
	45.0%	18.73%	5.57%	1.80%	0.59%	0.0%

Nusselt number on the top cover of the cavity Nu_{max}, it is necessary to use an order of magnitude more detailed grid with a step of 1/500. In other words, the estimate criterion must correspond the practical requirements of problem solution. If only the averaged characteristics are interesting, then the criterion can be an averaged value. Otherwise, it is necessary to select local flow and/or heat transfer characteristics as the criterion, including profiles of the corresponding heat and mass transfer parameters. In the latter case, as a consequence, a much more detailed grid will be required.

The results of the study of mixed fluid convection based on the Boussinesq approximation have been used for comparison due to the absence of the data from similar studies with an arbitrarily varying density in the literature. Isotherms and streamlines of fluid flow for mixed convection in a lid-driven square cavity at Pr = 0.7, Re = 1000, Ri = 1 in the case of Boussinesq approximation use are presented in Fig. 3 for these purposes. The reason for choosing these problem parameters was the fact that, as the literature analysis has showed, the most complex flow pattern was formed with these ones. As for the seemingly simple horizontal position of the isotherms, it is most convenient to compare the spatial positioning of similar lines of the liquid overheating in this case when matching different results. It can be seen that there is a good agreement between obtained results and literature data [Cheng, Liu, 2010].

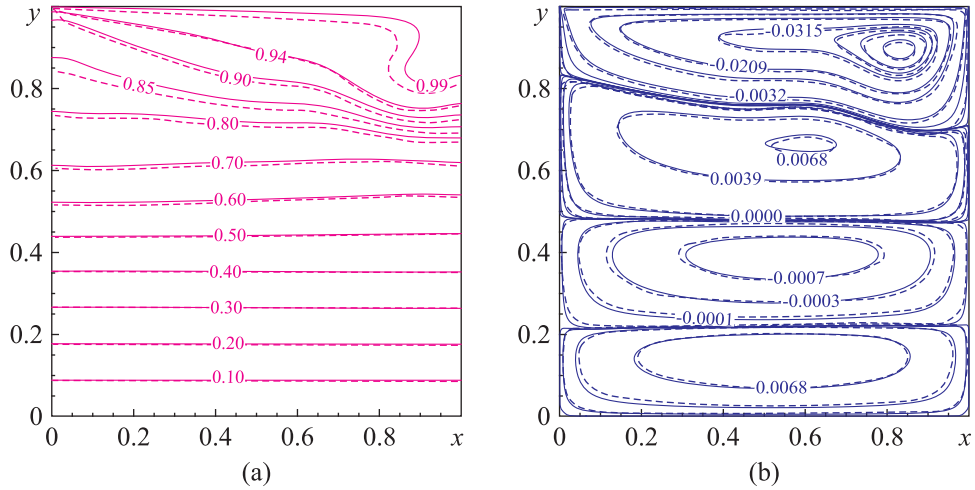

Figure 3. Comparison of present results (solid lines) with literature data (dashed lines, [Cheng, Liu, 2010]) for Re = 1000, Ri = 1, Pr = 0.7, and δ_T = 0 (Boussinesq approximation). Isolines of (a) relative overheating θ, (b) stream function

In conclusion, it should be mentioned that all calculations were carried out by the PC Intel Core i5-750, 2.66 GHz, RAM 12Gb. Typical solution time for a single task ranged from 4 to 8 hours, depending on a combination of the problem similarity parameters.

3. Computed results and discussion

3.1. Effect of buoyancy force on the flow map and heat transfer

In the problem statement under consideration, the buoyancy effect is determined by two parameters: the Richardson number Ri and the relative overheating of the cavity cover δ_T. This fact follows from the configuration of the mass force term of the motion equation for the vertical component of velocity (15). As mentioned above, the first of these two parameters plays the major role in determining the buoyancy effect, and the second parameter is an auxiliary one. However, the magnitude of δ_T also affects the inert properties of the stream as well. The work considers liquids of two viscosity levels: fluids with a relatively high viscosity (Re = 100) and vice versa, with a relatively

low one (Re = 1000). The Prandtl number in all calculations remains unchanged (Pr = 0.7), because the thermodynamic properties of the fluid are not the subject of consideration here.

The structures of 'cold' liquid flows (Ri = δ_T = 0) for two values of Reynolds number are shown in Fig. 4. These solutions are needful as a kind of reference point relative to which it is handily to analyze the effect of buoyancy force on the fluid flow and heat transfer.

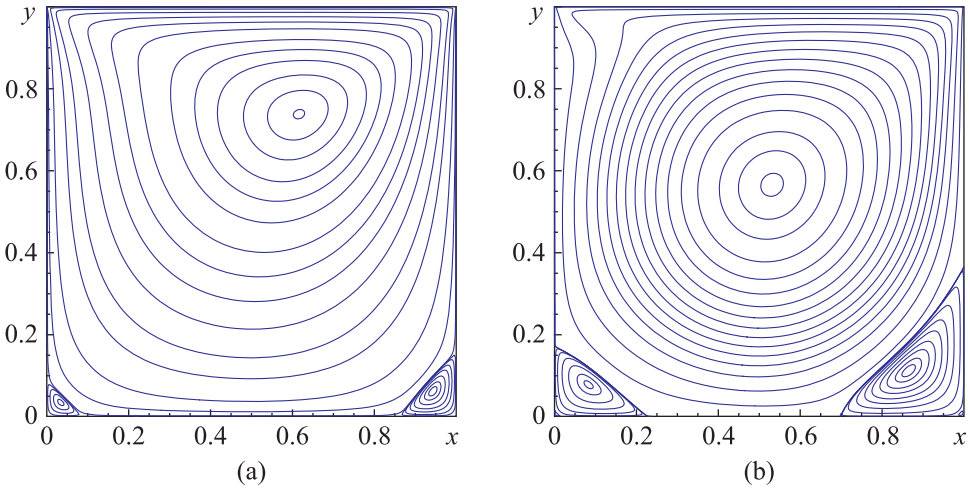

Figure 4. Flow map of the 'cold' liquid for (a) Re = 100, (b) Re = 1000

On the other hand, these calculations can be interpreted as additional validation of the program code due to the coincidence of flow patterns with classical results in the literature (see, for example, [Ghia et al., 1982; Isaev et al., 2002]). Comparison of fragments (a) and (b) of Fig. 4 indicates that lowering the liquid viscosity, ceteris paribus, causes the following consequences: 1) the center of rotation of the main vortex moves closer to the geometric center of the cavity and the vortex itself becomes more rounded in shape; 2) signs of the emergence of a new wall-adjacent vortex appear in the left-upper corner of the cavity; 3) the lower angular vortices increase in size.

The claimed study is logical to start with the analysis of the problem solution obtained in the framework of the Boussinesq approximation (Ri > 0, δ_T = 0). And since in this approximation the fluid density remains constant, this solution can also be considered as the second reference point in the study of fluid flows with variable density in the field of mass force. The structures of the flow and relative overheating fields at Re = 100 and various Richardson numbers are shown in Fig. 5. It is clear that the small Richardson number Ri = 0.1 causes the field of the streamlines to be almost the same as in the case of the motion of a 'cold' liquid (compare with Fig. 4, *a*).

A further increase in the number of Ri (an increase in the influence of buoyancy force) leads to the appearance of global vortices across the entire width of the cavity that move the liquid masses mainly in the horizontal direction. This change in the flow structure is explained by the increasing role of the buoyancy force, which prevents the penetration of warm fluid along the right wall of the cavity to its bottom. As a result, the liquid unfolds and moves from the right wall to the left one, followed by lifting to close the ring of circular motion. The greater the influence of the buoyancy force the earlier this turn of the fluid flow take place in the cavity height. The second vortex is generated under the first vortex due to the viscosity of the liquid. The driving force of the second vortex is the lower edge of the upper one just as for the upper vortex the driving force is the cover of the cavity. Further, the third vortex may arise under the second vortex, and so on. The greater the Richardson number is, the greater the number of transverse vortices will be. There are two vortices at Ri = 1 and as many as three ones at Ri = 10 in the cavity in the present case. As for the field of relative overheating, its structure becomes more and much simple as the Ri increases. Indeed, the isolation of fluid flows in transverse vortices

as the Richardson number increases does not promote the global convective heat transfer throughout the cavity region as it takes place in the case of Ri = 0.1. This fact is expressed in an almost uniform decrease in the temperature of the liquid from the cavity cover to its bottom for Ri = 10.

The results of solving exactly the same problem, but taking into account the variability of the liquid density (δ_T = 3) are presented in Fig. 6. Here the principal difference from the previous case is the presence of zones with both positive and negative buoyancy. These zones are separated by a dashed line of zero buoyancy for which the condition $\rho = \rho_a \equiv 1$ is satisfied.

Despite this difference the fields of relative overheating for these two cases are very similar for all values of the Richardson number. Changes in the pattern of fluid flow have occurred, but not for all Ri values. At Ri = 0.1 streamlines are almost the same as for Boussinesq approximation case (see Fig. 5, *a*). While the changes in flow structures with the growth of the Richardson number resemble similar changes in Fig. 5, but they are expressed noticeable weaker. It is not difficult to see in Fig. 6, *b*, that although the lower vortex has already formed, its structure is a some average between a completely horizontal vortex and two separate angular vortices. Similarly, only two horizontal vortices are present in fragment (*c*) of Fig. 6 instead of three ones, as it is for the case with the Boussinesq approximation (compare with Fig. 5, *c*).

Attention should also be paid to the shape of the zero buoyancy curve in Fig. 6. It has a pronounced curved appearance in the first two fragments of the figure. This is due to the provision of heat transfer by the global vortex of liquid circulation. The deep penetration of the warm liquid downwards along the right wall of the cavity causes lowering of the right part of the zero buoyancy line. Likewise, but on the contrary, the mechanism for raising the left side of the zero buoyancy line

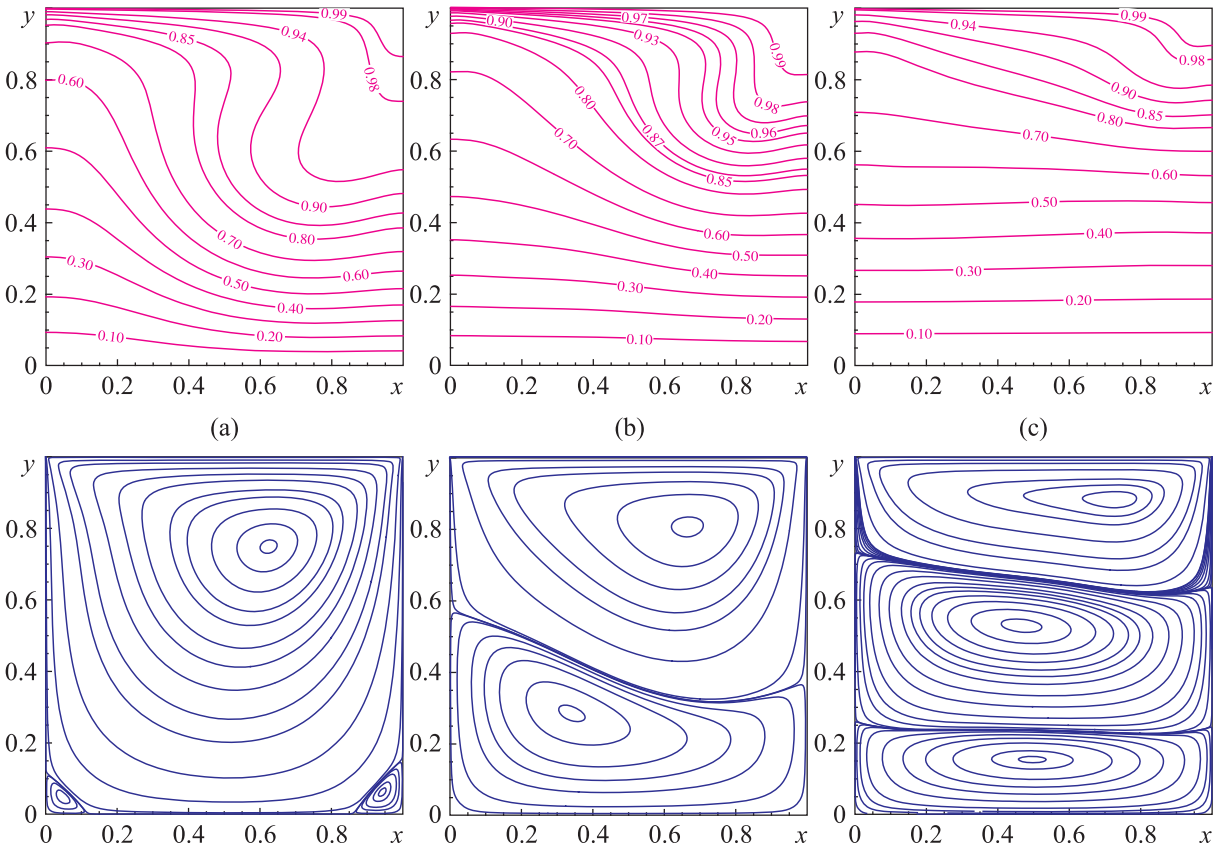

Figure 5. Isolines of relative overheating θ (top row) and streamlines (bottom row) for Re = 100, δ_T = 0 (Boussinesq approximation): (a) Ri = 0.1, (b) Ri = 1, (c) Ri = 10

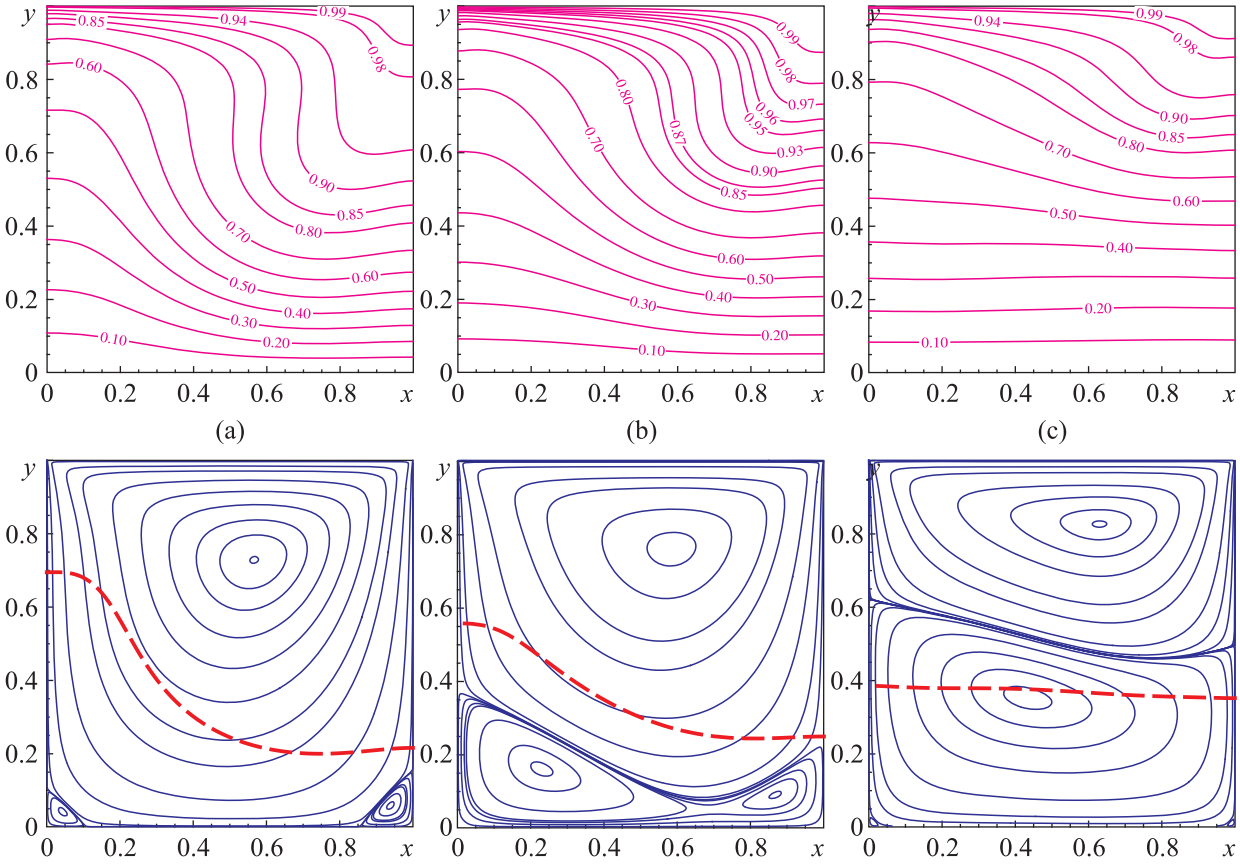

Figure 6. Isolines of relative overheating θ (top row) and streamlines (bottom row) for Re = 100, δ_T = 3: (a) Ri = 0.1, (b) Ri = 1, (c) Ri = 10. Dashed line is the zero buoyancy one

works: the lower cooled portions of the liquid rise upward along the left cavity wall with the same global vortex. In the third fragment (*c*) of Fig. 6 the heat is transferred vertically mainly due to thermal conductivity by virtue of the isolation of convective heat transfer because of the formation of two horizontal vortices one above the other. As a consequence, the zero buoyancy line is almost a horizontal line segment for this case. It is easy to understand that since the fluid density is a function only of the liquid overheating (see (17)), the line of zero buoyancy always coincides with the isotherm $\theta = \theta_a$. The behavior of the isotherms of the relative overheating in the top row of the figure confirms this conclusion.

Profiles of velocity components $u(y)$ and $v(x)$ along the lengthwise and crosswise sections of the cavity for different values of the Richardson number and the relative overheating of the cover are presented in Fig. 7. It is well seen that taking into account the density variability leads, if not to fundamental, then at least noticeable changes in the profiles.

It should also be noted that the volatility of the horizontal velocity component u decreases at the bottom part of the cavity as the number Ri increases. In other words, the kinetic energy of fluid motion is mainly concentrated in the upper half of the cavity as the effects of buoyancy increase, regardless of what level approximation is used to describe mixed-type convection of liquid.

A similar series of solutions but at Re = 1000 was obtained in order to evaluate the effect of viscosity on heat and mass transfer of the liquid in the problem under consideration. The Boussinesq approximation is considered at the beginning stage of the study (Fig. 8) as it was in the previous case at Re = 100 (Fig. 5). At first glance, similar conclusions can be drawn from the pictures of heat and mass transfer as in the case of a flow with increased viscosity. As before, there is almost the coincidence

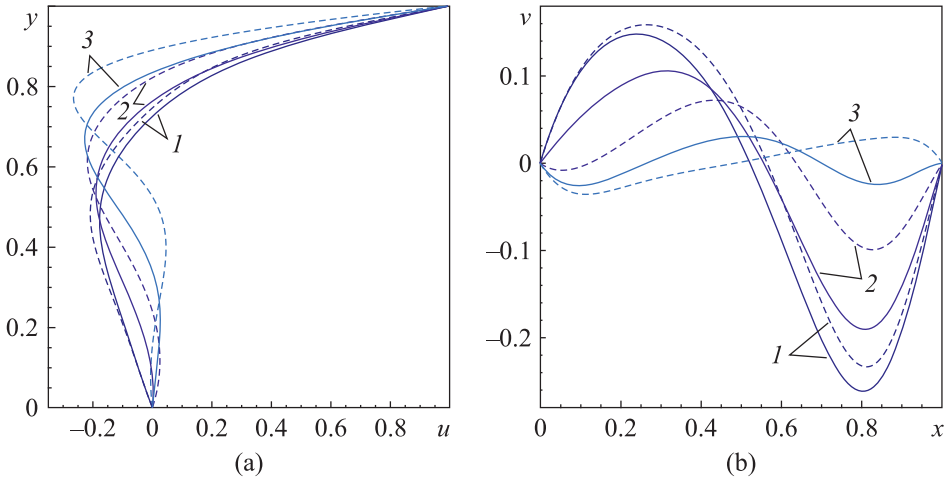

Figure 7. Profiles of components of the velocity vector for Re = 100: (a) $u(y)$ at $x = 0.5$, (b) $v(x)$ at $y = 0.9$; 1 — Ri = 0.1, 2 — Ri = 1, 3 — Ri = 10; $\delta_T = 0$ (Boussinesq approximation) — dashed lines, $\delta_T = 3$ — solid lines

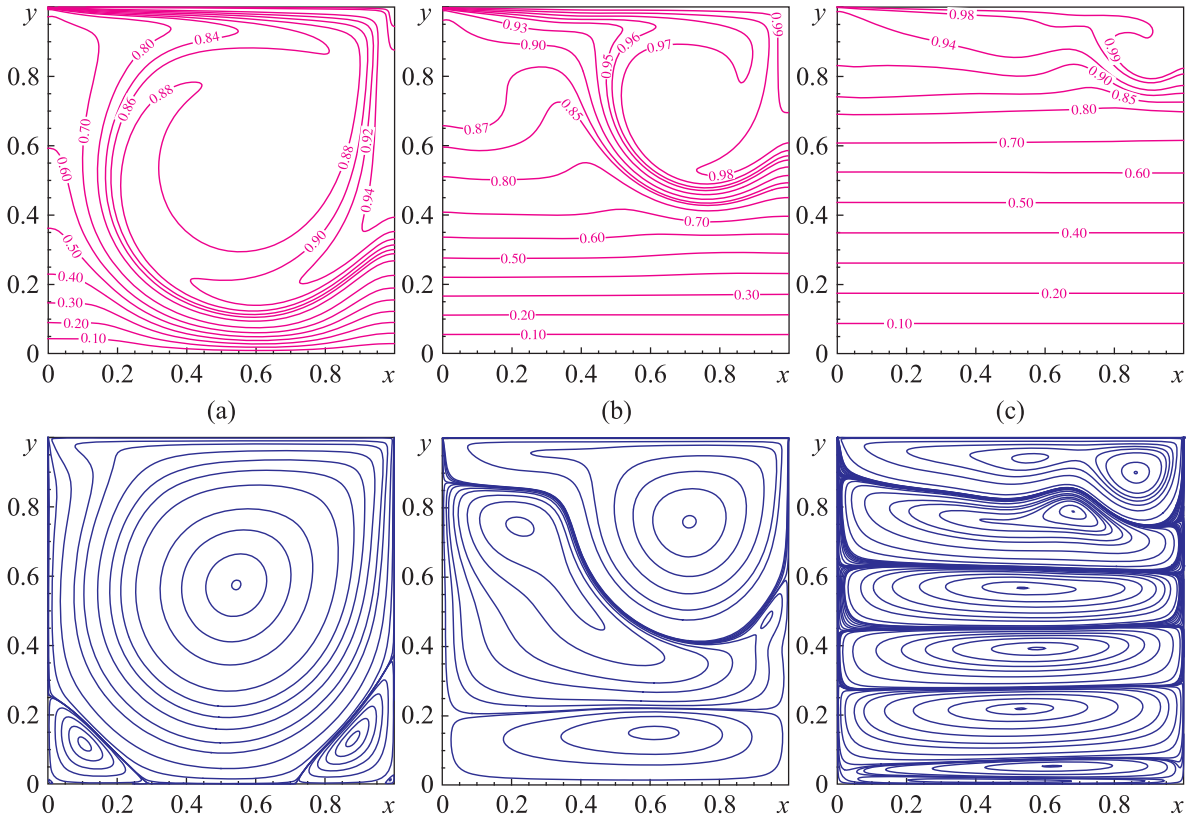

Figure 8. Isolines of relative overheating θ (top row) and streamlines (bottom row) for Re = 1000, $\delta_T = 0$ (Boussinesq approximation): (a) Ri = 0.1, (b) Ri = 1, (c) Ri = 10

of flow structures at Ri = 0.1 and 'cold' fluid takes place (compare Fig. 4, *b* and Fig. 8, *a*). Again, transverse vortices arise, the number of which increases as the influence of buoyancy forces increases.

However, there are also serious differences in the structures of heat transfer and fluid flow here. Briefly, these differences can be characterized as an increase in separateness of individual areas of heat and mass transfer. First, there is practically no area of uniform temperature drop from top to bottom in the pattern of isotherms of the relative overheating (Fig. 8, *a*). The central region of strongly

swirled isotherms, which repeats the major vortex in its position and size, indicates a pronounced predominance of the convective heat transfer mechanism. Second, there is a sharp boundary between the swirling isotherms at the top of the cavity and the set of horizontal isotherms at its bottom. Third, only one lower vortex of the three global vortices at Ri = 1 can be characterized as a horizontal one. While the upper vortex in Fig. 8, *b* continues to preserve the properties of the central vortex in Fig. 8, *a*, but on a reduced scale. And, finally, fourthly, the number of horizontal vortices at Ri = 10 (complete dominance of buoyancy forces) has doubled from three to six (compare with Fig. 5, *c*).

The results of further complication of the problem, taking into account the density variability (δ_T = 3) for low viscosity fluid, are presented in Fig. 9. First of all, the patterns of the flow and relative overheating at Ri = 1 attract attention (Fig. 9, *b*). It seems that the variability in density, as it were, further reduces the viscosity of the liquid. Although by the condition of the problem, the viscosity is considered constant. The effect of an additional decrease in viscosity is expressed, in particular, in the increased size of both the central vortex and the region of almost uniform heating in the center of the cavity, which corresponds to this vortex. This is also evidenced by the increase in the degree of isolation of different sections of the flow, which is expressed in an increase in the number of large and medium vortices in Fig. 9, *b*. On the other hand, it should also be noted that the number of transverse vortices decreased from six to five ones for Ri = 10. Moreover, the upper vortex in Fig. 9, *c* can be hardly considered as a transverse one.

The consequence of the reduced viscosity of the liquid is a large curvature of the zero buoyancy line at Ri = 0.1. Its position in space indicates that the rotation of the central vortex is slowed down by the volumetric buoyancy force not only on the right vortex side where the fluid falls down but also partially on the left side of the vortex near the left wall of the cavity. In other words, in a relative sense,

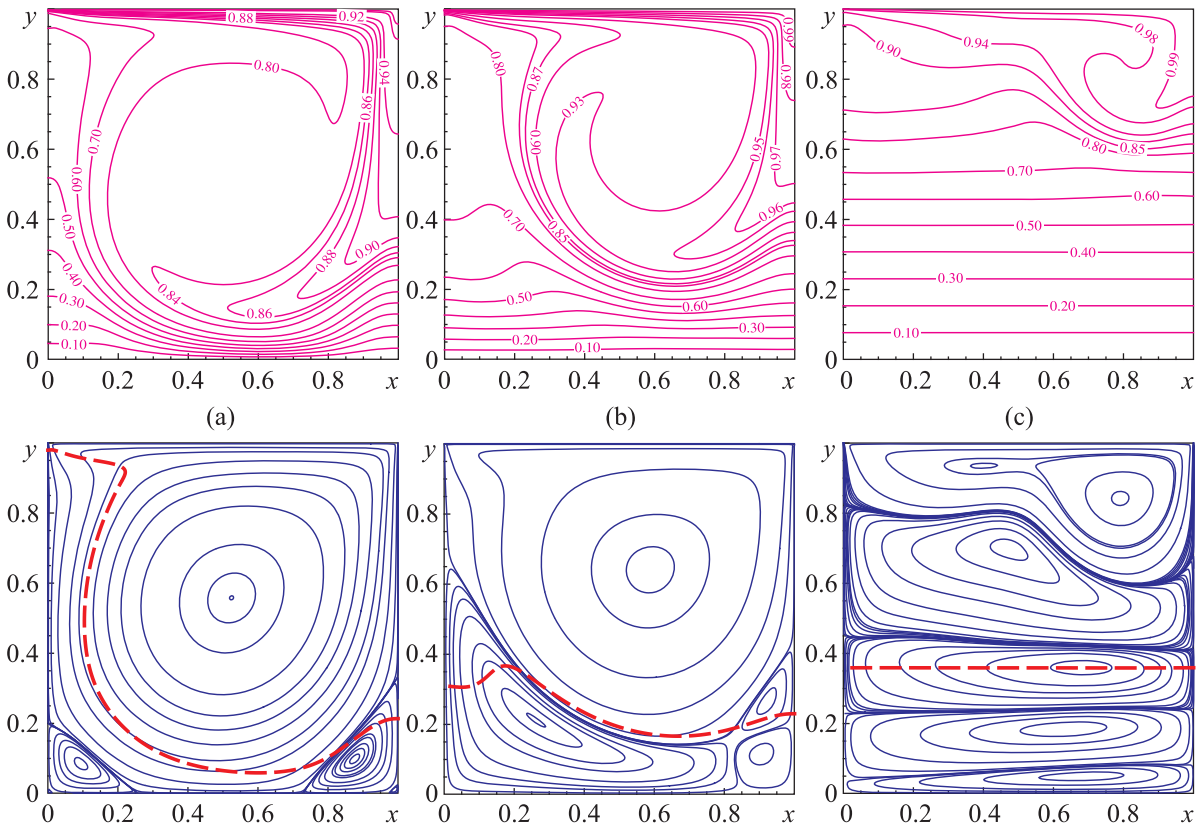

Figure 9. Isolines of relative overheating θ (top row) and streamlines (bottom row) for Re = 1000, δ_T = 3: (a) Ri = 0.1, (b) Ri = 1, (c) Ri = 10. Dashed line is the zero buoyancy one

the rotation of the fluid is delayed by the buoyancy forces to a greater measure than when modeling mixed convection in the framework of the Boussinesq approximation where buoyancy is positive in the entire flow region. This effect of additional braking of the liquid rotation occurs because of the presence of a vertical section of the zero buoyancy line near the left wall of the cavity. In this case there is a violation of the symmetry of the effect of the buoyancy force on the opposite parts of the vortex in the direction of immersion/emersion of the liquid. On the contrary, the more or less horizontal arrangement of the zero buoyancy lines in Fig. 9, *b*, *c* informs that in these cases the buoyancy force performs exactly the same role of acceleration and deceleration of the flow as when the Boussinesq approximation is used.

As in the previous case for Ri = 100, profiles of velocity components $u(y)$ and $v(x)$ along the lengthwise and crosswise sections of the cavity are presented in Fig. 10 in order to estimate the quantitative characteristics of fluid movement. It is well seen that the maximum differences in the graphs of the velocity components for the cases of the Boussinesq approximation and the variable density of the liquid are achieved at Ri = 1 (curves 2 in the figure), that is when inertia and buoyancy of the flow are approximately equal to each other. While in the case of high fluid viscosity, the maximum difference between the respective profiles occurs at Ri = 10, the minimum one — at Ri = 0.1 (see Fig. 7). It should also be noted that the fluid motion gradually decays in the lower half of the cavity as the influence of buoyancy forces increases (the number Ri increases) and almost all kinetic energy of the flow is concentrated in the upper part of the cavity. This conclusion follows from the vertical behavior of the $u(y)$ profiles of curves 3 and partly of curves 2 near the zero mark in Fig. 10, *a*. And also it follows from the flow structure in Fig. 9, *c* where the liquid can not accelerate vertically in the narrow horizontal vortices of the lower half of the cavity in principle.

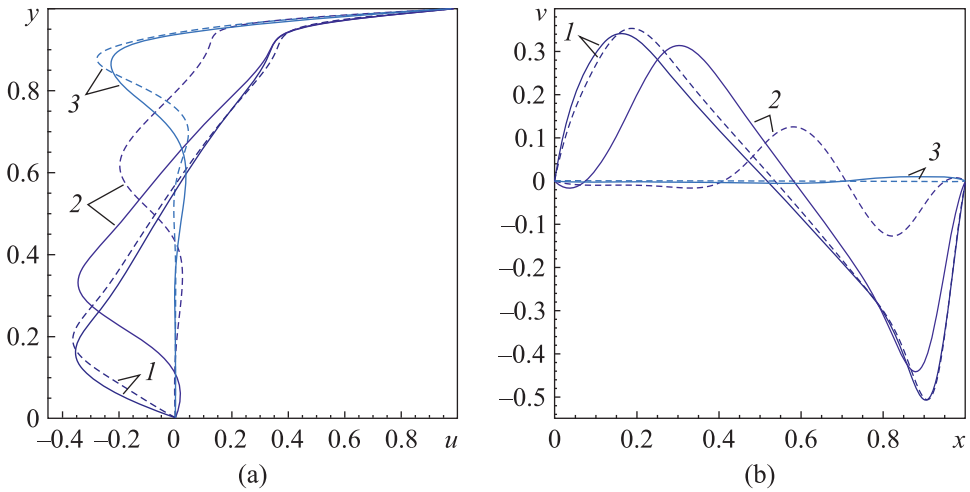

Figure 10. Profiles of components of the velocity vector for Re = 1000: (a) $u(y)$ at $x = 0.5$, (b) $v(x)$ at $y = 0.9$; 1 — Ri = 0.1, 2 — Ri = 1, 3 — Ri = 10; $\delta_T = 0$ (Boussinesq approximation) — dashed lines, $\delta_T = 3$ — solid lines

3.2. Heat exchange and flow friction on the bottom cavity wall

Special attention should be paid to the characteristics of friction and heat exchange on the cavity walls because these characteristics are the most important in practical studies. Graphs of the Nusselt number Nu along the bottom wall of the cavity for different values of the similarity parameters Re, Ri, and δ_T are shown in Fig. 11. It is not difficult to see that the values of the number Nu are negative for all situations under consideration. This is explained by the direction of the heat flow from the fluid to the wall, that is, in the opposite direction with respect to the external normal to the inner surface of the cavity bottom. The first thing that attracts attention is the similarity of the curves and even their

almost coincidence for the case of highly viscous liquids (Re = 100) at a weak influence of buoyancy forces (Ri = 0.1, see Fig. 11, *a*). A further increase in the influence of buoyancy forces causes a good separability of the Nu number curves. It is characteristic, that large absolute values of Nu are achieved at large values of relative overheating δ_T regardless of the degree of the fluid viscosity. A small exception to this rule is contained in the top part of the fragment (*b*) of Fig. 11, where, curiously, all the curves of Nu are intersected at almost the same point. And one more point to which it is necessary to pay attention. The maximum absolute value of the dimensionless heat flux is achieved in the case of a low-viscosity fluid (Re = 1000) with the predominance of convective transport over buoyancy (Ri = 0.1). Which is to be expected on the basis of the most compact arrangement of the isolines of relative overheating (see Fig. 9, *a*) in the immediate vicinity of the cavity bottom. Further, the maximum of the Nu number modulo steadily decreases as the Ri number increases (see fragments (*b*) and (*c*) in Fig. 11).

Same as previous, profiles of the modified coefficient of friction C_f^* along the bottom wall of the cavity for different values of Re, Ri, and δ_T are presented in Fig. 12. Here, as well as for the Nu number, there is a similarity or even coincidence of the C_f^* graphs for the case of a weak influence of buoyancy forces (Ri = 0.1). However, in contrast to the behavior of the Nu number graphs, it cannot be stated here that the maximum of C_f^* modulus is reached at the maximum value of δ_T. Moreover, the sign of the modified coefficient of friction changes not only from Re, Ri, and δ_T, but also from the value of the spatial coordinate x (see fragment (*a*) and the bottom part of fragment (*b*) of Fig. 12). The reason for this is the structure of the flow highly dependent on the problem parameters. Namely, how many vortices are in the bottom layer of the stream, in which direction they rotate, and at what speed the fluid moves along the wall. However, there is a general trend in the behavior of the modified coefficient of friction: as the number Ri increases, the absolute value of C_f^* decreases. Herewith, this decrease is more intense for a less viscous liquid. So, the value of the coefficient C_f^* for Re = 100

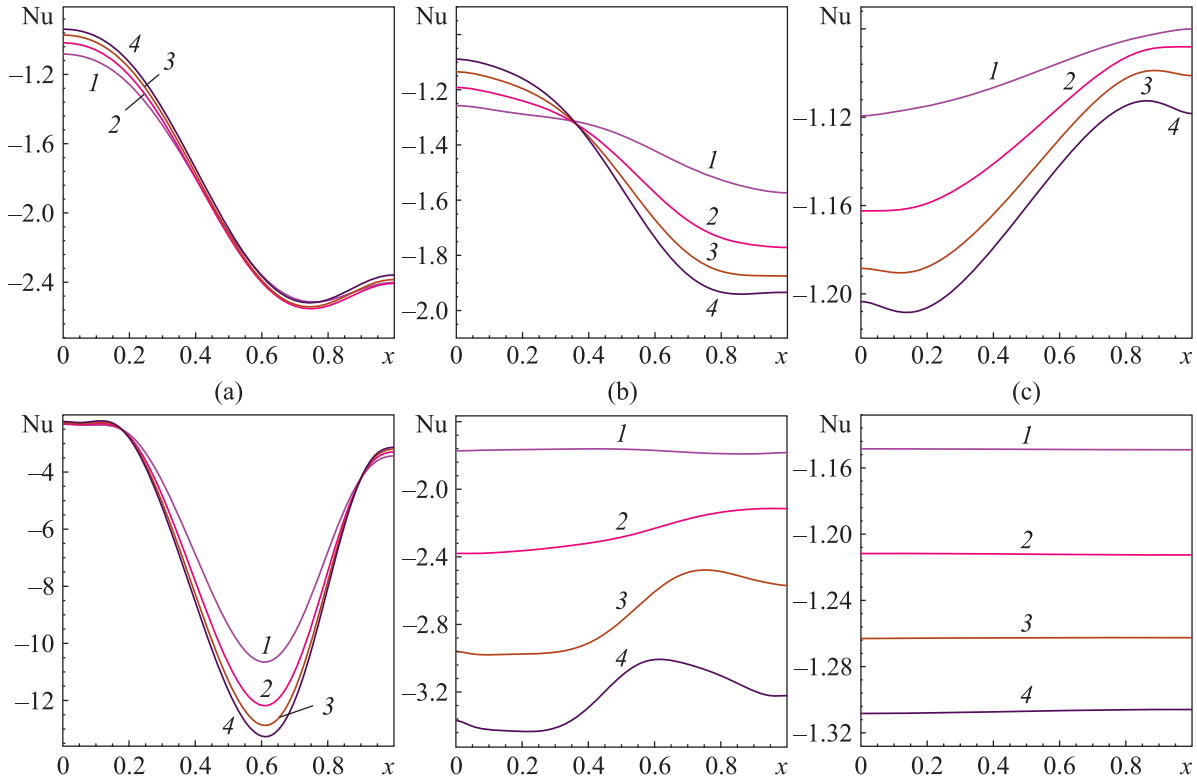

Figure 11. Nusselt number on the bottom cavity wall for Re = 100 (top row) and Re = 1000 (bottom row): (a) Ri = 0.1, (b) Ri = 1, (c) Ri = 10; 1 — δ_T = 0, 2 — δ_T = 1, 3 — δ_T = 2, 4 — δ_T = 3

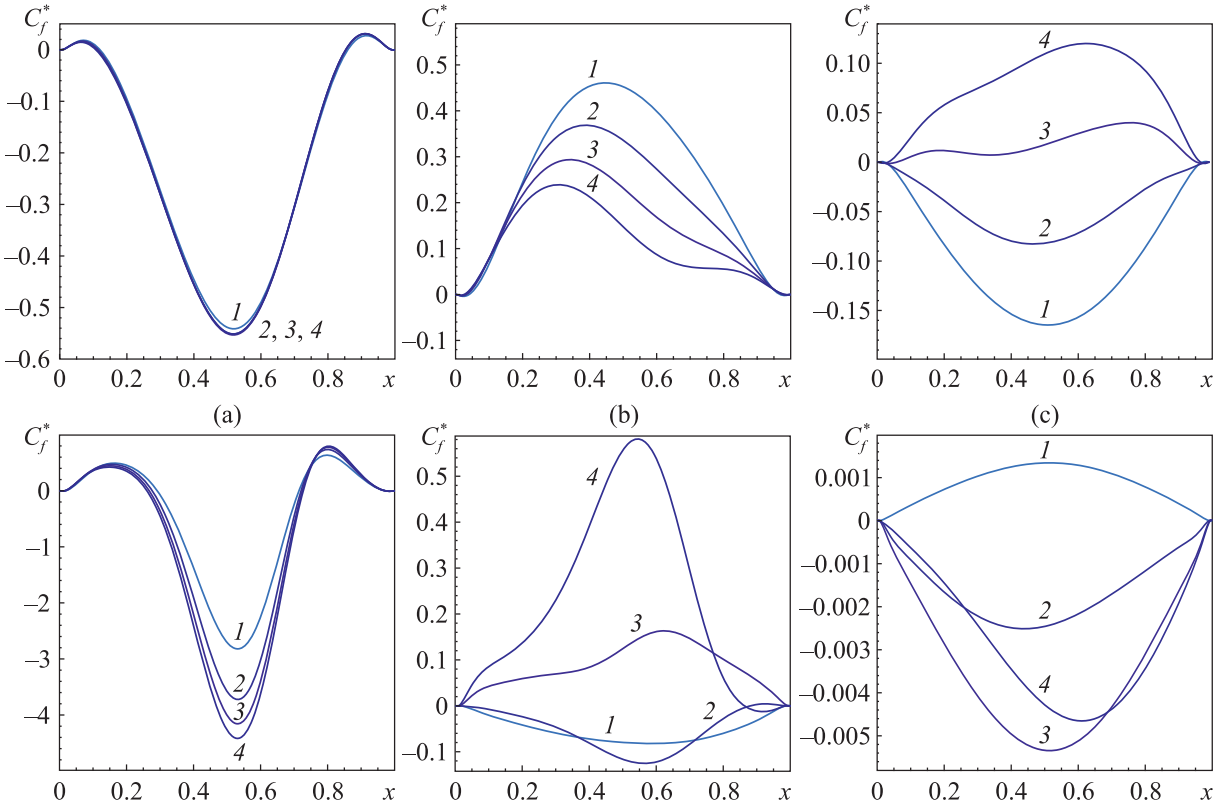

Figure 12. Flow friction on the bottom cavity wall for Re = 100 (top row) and Re = 1000 (bottom row): (a) Ri = 0.1, (b) Ri = 1, (c) Ri = 10; 1 — δ_T = 0, 2 — δ_T = 1, 3 — δ_T = 2, 4 — δ_T = 3

with an increase in Ri from 0.1 to 100 decreased by no more than an order of magnitude. While for Re = 1000, the value of C_f^* modulo decreased by three orders of magnitude under the same conditions.

Conclusion

Results of numerical solutions of the stationary incompressible flow of viscous heat-conducting liquid with variable density in the 2D lid-driven square cavity with heated top cover in the field of mass force are contained in the article. The aim of the study was to determine the influence of buoyancy force on the nature of the flow and heat transfer during mixed convection in the device under consideration. The investigations have been carried out for the following values of similarity parameters: Prandtl number Pr = 0.70; Reynolds number Re = 100 and 1000; Richardson number Ri = 0.1, 1, and 10; relative overheating of the cavity cover δ_T = 0, 1, 2, and 3. The validation of the solution has been fulfilled by comparison with the literature data for the case of the Boussinesq approximation. The comparative analysis of two-dimensional fields of streamlines and isotherms of relative overheating has been presented in the article for the above problem parameters. Profiles of velocity components, Nusselt number Nu, and modified coefficient of friction C_f^* have been considered in different sections of the cavity.

The following conclusions can be formulated as a result of this study.

1. An increase in the Richardson number leads to appearance of horizontal vortices in the entire cavity width, the number of which grows with increasing values of Re and Ri.

2. An increase in the influence of buoyancy forces leads to the formation of a zone of uniform heating in the cavity width, the temperature in which is almost linearly reduced from the upper layers

of the zone to the cavity bottom. The height of the zone increases as the Ri number increases and/or the Re number decreases.

3. The concentration of kinetic energy of fluid motion takes place in the upper part of the cavity directly under the moving lid as the Ri number increases.

4. Taking into account the variability of the fluid density causes a weakening of the effect of buoyancy force on the transformation of flow structures and fluid heating in the cavity.

5. An increase in the Richardson number Ri causes a decrease in the absolute values of the Nusselt number Nu and the modified coefficient of friction C_f^*. On the other hand, the increase in the relative overheating of the cover δ_T leads to an increase in the Nu number modulus. As for C_f^*, it can both increase and decrease as δ_T increases.

References

Abu-Nada E., Al-Sarkhi A., Akash B., Al-Hinti I. Heat transfer and fluid flow characteristics of separated flows encountered in a backward–facing step under the effect of suction and blowing // Journal of Heat Transfer. — 2007. — Vol. 129, No. 11. — P. 1517–1528. — DOI: 10.1115/1.2759973

Armengol J. M., Bannwart F. C., Xaman J., Santos R. G. Effects of variable air properties on transient natural convection for large temperature differences // International Journal of Thermal Sciences. — May 2017. — DOI: 10.1016/j.ijthermalsci.2017.05.024

Becker R., Braack M. Solution of a stationary benchmark problem for natural convection with large temperature difference // International Journal of Thermal Sciences. — 2002. — Vol. 41, Iss. 5. — P. 428–439. — DOI: 10.1016/S1290-0729(02)01335-2

Belotserkovskii O. M., Gushchin V. A., Shchennikov V. V. Use of the splitting method to solve problems of the dynamics of a viscous incompressible fluid // USSR Computational Mathematics and Mathematical Physics. — 1975. — Vol. 15, No. 1. — P. 190–200. — DOI: 10.1016/0041-5553(75)90146-9

Cheng T. S., Liu W.-H. Effect of temperature gradient orientation on the characteristics of mixed convection flow in a lid–driven square cavity // Computers & Fluids. — 2010. — Vol. 39, Iss. 6. — P. 965–978. — DOI: 10.1016/j.compfluid.2010.01.009

Cheng T. S. Characteristics of mixed convection heat transfer in a lid–driven square cavity with various Richardson and Prandtl numbers // International Journal of Thermal Sciences. — 2011. — Vol. 50, Iss. 2. — P. 197–205. — DOI: 10.1016/j.ijthermalsci.2010.09.012

Fomin A. A., Fomina L. N. Numerical solution of the problem of incompressible fluid flow in a plane channel with a backward–facing step at high Reynolds numbers // Journal of Applied Mechanics and Technical Physics. — 2018. — Vol. 59, No. 7. — P. 1211–1226. — DOI: 10.1134/S0021894418070052

Ghia U., Ghia K. N., Shin C. T. High–Re solutions for incompressible flow using the Navier–Stokes equations and a multigrid method // Journal of Computational Physics. — 1982. — Vol. 48, No. 3. — P. 387–411. — DOI: 10.1016/0021-9991(82)90058-4

Isaev S. A., Sudakov A. G., Luchko N. N., Sidorovich T. V. Numerical modeling of laminar circulation flow in a square cavity with a moving boundary at high Reynolds number // Journal of Engineering Physics and Thermophysics. — 2002. — Vol. 75, No. 1. — P. 71–80. — DOI: 10.1023/A:1014814622200

Iwatsu R., Hyun J. M., Kuwahara K. Mixed convection in a driven cavity with a stable vertical temperature gradient // International Journal of Heat and Mass Transfer. — 1993. — Vol. 36, Iss. 6. — P. 1601–1608. — DOI: 10.1016/S0017-9310(05)80069-9

le Quere P., Weisman C., Paillere H., Vierendeels J., Dick E., Becker R., Braack M., Locke J. Modelling of natural convection flows with large temperature differences: a benchmark problem for low mach number solvers. Part 1. Reference solutions // ESAIM: Mathematical Modelling and Numerical Analysis. — 2005. — Vol. 39, No. 3. — P. 609–616. — DOI: 10.1051/m2an:2005027

Loitsyanskiy L. G. Mechanics of liquids and gases. — NY: Begell House, 1995.

Luo W.-J., Yang R.-J. Multiple fluid flow and heat transfer solutions in a two–sided lid–driven cavity // International Journal of Heat and Mass Transfer. — 2007. — Vol. 50, Iss. 11–12. — P. 2394–2405. — DOI: 10.1016/j.ijheatmasstransfer.2006.10.025

Oztop H. F., Dagtekin I. Mixed convection in two-sided lid-driven differentially heated square cavity // International Journal of Heat and Mass Transfer. — 2004. — Vol. 47, Iss. 8–9. — P. 1761–1769. — DOI: 10.1016/j.ijheatmasstransfer.2003.10.016

Patankar S. V. Numerical heat transfer and fluid flow. — NY: Hemisphere Publ. Corp., 1980. — 197 p.

Sivakumar V., Sivasankaran S., Prakash P., Lee J. Effect of heating location and size on mixed convection in lid–driven cavities // Computers & Mathematics with Applications. — 2010. — Vol. 59, Iss. 9. — P. 3053–3065. — DOI: 10.1016/j.camwa.2010.02.025

Sun H., Lauriat G., Sun D. L., Tao W. Q. Transient double–diffusive convection in an enclosure with large density variations // International Journal of Heat and Mass Transfer. — 2010. — Vol. 53, Iss. 4. — P. 615–625. — DOI: 10.1016/j.ijheatmasstransfer.2009.10.035

Кузнецов Г. В., Максимов В. И. Численное исследование влияния условий неоднородного теплообмена на смешанную конвекцию в прямоугольной области с локальными источниками ввода и вывода массы // Известия Российской академии наук. Энергетика. — 2008. — № 4. — С. 112–118.
Kuznetsov G. V., Maximov V. I. Chislennoe issledovanie vliyaniya uslovii neodnorodnogo teploobmena na smeshannuyu konvektsiyu v pryamougol'noi oblasti s lokal'nymi istochnikami vvoda i vyvoda massy [Numerical study of the influence of inhomogeneous heat transfer conditions on mixed convection in a rectangular region with local sources of mass input and output] // Thermal Engineering. — 2008. — No. 4. — P. 112–118 (in Russian).

Малышев В. Л., Моисеев К. В., Моисеева Е. Ф. Режимы течения слоя жидкости при смешанной конвекции // Труды Института механики Уфимского научного центра РАН. — 2011. — Т. 8, № 1. — С. 124–132.
Malyshev V. L., Moiseev K. V., Moiseeva E. F. Rezhimy techeniya sloya zhidkosti pri smeshannoi konvektsii [The modes of flow of a liquid layer in mixed convection] // Proceedings of the Mavlyutov Institute of Mechanics. — 2011. — Vol. 8, No. 1. — P. 124–132. — DOI: 10.21662/uim2011.1.011 (in Russian).

Михайленко С. А., Шеремет М. А. Моделирование конвективно-радиационного теплопереноса в дифференциально обогреваемой вращающейся полости // Компьютерные исследования и моделирование. — 2018. — Т. 10, № 2. — С. 195–207.
Mihailenko S. A., Sheremet M. A. Modelirovanie konvektivno–radiatsionnogo teploperenosa v differentsial'no obogrevaemoi vrashchayushcheisya polosti [Simulation of convective-radiative heat transfer in a differentially heated rotating cavity] // Computer research and modeling. — 2018. — Vol. 10, No. 2. — P. 195–207. DOI: 10.20537/2076-7633-2018-10-2-195-207 (in Russian).

Нехамкина О. А., Никулин Д. А., Стрелец М. Х. Об иерархии моделей тепловой естественной конвекции совершенного газа // Теплофизика высоких температур. — 1989. — Т. 27, вып. 6. — С. 1115–1125.
Nehamkina O. A., Nikulin D. A., Strelets M. H. Ob ierarkhii modelei teplovoi estestvennoi konvektsii sovershennogo gaza [On the hierarchy of models of thermal natural convection of a perfect gas] // High Temperature. — 1989. — Vol. 27, Iss. 6. — P. 1115–1125 (in Russian).

Фомин А. А., Фомина Л. Н. Ускорение полинейного рекуррентного метода в подпространствах Крылова // Вестник Томского государственного университета. Математика и механика. — 2011. — Т. 14, № 2. — С. 45–54.
Fomin A. A., Fomina L. N. Uskorenie polineinogo rekurrentnogo metoda v podprostranstvakh Krylova [Acceleration of the line-by-line recurretnt method in Krylov subspaces] // Tomsk State University Journal of Mathematics and Mechanics. — 2011. — Vol. 14, No. 2. — P. 45–54 (in Russian).

Фомин А. А., Фомина Л. Н. Неявный итерационный полинейный рекуррентный метод в применении к решению задач динамики несжимаемой вязкой жидкости // Компьютерные исследования и моделирование. — 2015. — Т. 7, № 1. — С. 35–50.

Fomin A. A., Fomina L. N. Neyavnyi iteratsionnyi polineinyi rekurrentnyi metod v primenenii k resheniyu zadach dinamiki neszhimaemoi vyazkoi zhidkosti [The implicit line-by-line recurrence method in application to the solution of problems of incompressible viscous fluid dynamics] // Computer Research and Modeling. — 2015. — Vol. 7, No. 1. — P. 35–50. — DOI: 10.20537/2076-7633-2015-7-1-35-50 (in Russian).

Фомин А. А., Фомина Л. Н. О сходимости неявного итерационного полинейного рекуррентного метода решения систем разностных эллиптических уравнений // Компьютерные исследования и моделирование. — 2017. — Т. 9, № 6. — С. 857–880.

Fomin A. A., Fomina L. N. O skhodimosti neyavnogo iteratsionnogo polineinogo rekurrentnogo metoda resheniya sistem raznostnykh ellipticheskikh uravnenii [On the convergence of the implicit iterative line-by-line recurrence method for solving difference elliptical equations] // Computer Research and Modeling. — 2017. — Vol. 9, No. 6. — P. 857–880. — DOI: 10.20537/2076-7633-2017-9-6-857-880 (in Russian).